https://doi.org/10.61092/iaea.6t0c-exk2

INDC(NDS)-0903

IAEA
International Atomic Energy Agency

INDC International Nuclear Data Committee

Revisiting the upbend in the (n,γ) photon strength function data of ^{57}Fe

Prepared by

Jiri Kopecky
JUKO Research
Alkmaar, The Netherlands

Ivo Tomandl
Nuclear Physics Institute
CAS Řež, Czech Republic

August 2024

IAEA Nuclear Data Section

Vienna International Centre, P.O. Box 100, 1400 Vienna, Austria

INDC documents may be downloaded in electronic form from

http://nds.iaea.org/publications.

Requests for hardcopy or e-mail transmittal should be directed to

NDS.Contact-Point@iaea.org

or to:

Nuclear Data Section
International Atomic Energy Agency
Vienna International Centre
PO Box 100
1400 Vienna
Austria

INDC(NDS)-0903
Distr. G,NM,PH

Revisiting the upbend in the (n,γ) photon strength function data of ^{57}Fe

Prepared by

Jiri Kopecky
JUKO Research
Alkmaar, The Netherlands

Ivo Tomandl
Nuclear Physics Institute
CAS Řež, Czech Republic

August 2024

Contents

1. Introduction

Photon strength functions (PSF) form the basic input information for theoretical models describing the gamma decay in nuclear reactions and constitute a segment of the Reference Input Parameter Library [https://www.nds.iaea.org/ripl/]. Recently, the IAEA NDS has completed a CRP on Generating a Reference Database for Photon Strength Functions with the aim to produce a PSF database comprising all available experimental PSF data. Results of the CRP have been documented in Ref. [1] and the PSF database is available on the IAEA website [https://www.nds.iaea.org/PSFdatabase].

The "upbend" or low energy enhancement (LEE), namely, the enhanced gamma-ray strength at very low transition energies above the widely accepted statistical manner of the nucleus de-excitation was introduced in 2004 by the OSLO group. In the first publication claiming this effect for the PSF, the ^{57}Fe(^{3}He,^{3}He'γ)^{57}Fe and ^{57}Fe(^{3}He,$\alpha\gamma$)^{56}Fe reactions were used [2, 3], while in later works (p,p') measurements were used [4, 5]. For simplification, we shall denote such experiments as the "Oslo method", as has also been recently adopted in the literature. Similar PSF data, in both magnitude and shape, have been recognized in Ref. [3] and can be used as an additional information.

The main aim of this work is to explore some advantages of neutron capture measurements, in terms of the experimental simplicity and model-independent way of extracting the information on the low-lying strength. While in neutron capture the initial nuclear states that are excited have known spins and parities, the Oslo measurements define the energy E_i bins with undefined spin and parity resulting in unknown transition multipolarity. Although the latter is assumed to be of dipole nature, the excited levels in the bin may have spin windows different to those in the capture reaction. This fact may complicate the issue of compatibility of the capture and Oslo data.

The report is divided into 3 sections, the ^{56}Fe(n,γ)^{57}Fe analysis and data from Refs [6, 7], the low-energy secondary capture estimates, and the comparison with ^{57}Fe PSF data from other experiments. The analysis is based on experimental results without any additional theoretical simulations. The data from Ref. [7] are further denoted to its origin as BRR (the Budapest Research reactor). The main aim of this work was to unite all available neutron capture information on the compound nucleus ^{57}Fe and give a detailed comparison of the capture and Oslo measurements.

2. The ^{56}Fe neutron capture reaction

2.1. Thermal capture

2.1.1. The statistical model

The thermal capture (THC) data from the ECN analysis [6] and the recent data from the BRR/UJF collaboration [7] have been compared in Ref. [8] (collaboration between Budapest Research Reactor and UJF Rez). The Discrete Resonance Capture (DRC) data from the p-wave capture measurement at E_n = 1.147 keV (see Ref. [9]) has also been included to test the absolute normalization of these three independent measurements, which is important for validating the derived absolute calibration of the PSF values. An overview of these measurement parameters is given in Table 1 and the resulting PSF values for primary transitions are plotted in Fig.1 for both THC measurements.

TABLE 1. Comparison of the beam/target situation and the number of detected transitions, as total number of transitions assigned in the decay scheme (#gammas), number of primary, secondary, and unassigned transitions (prim, sec and unass), respectively. Finally, the last column gives the number of total transitions of the decaying ^{57}Fe nucleus.

Laboratory	n-beam	target	# gammas	#prim	#sec	#unass	#tot
BNL	1.147 keV	91.8%nat	19	19			19
ECN 1980	thermal	91.8%nat	191	33	58	62	253
BRR 2017	thermal	99.94%	453	88	365	19	472

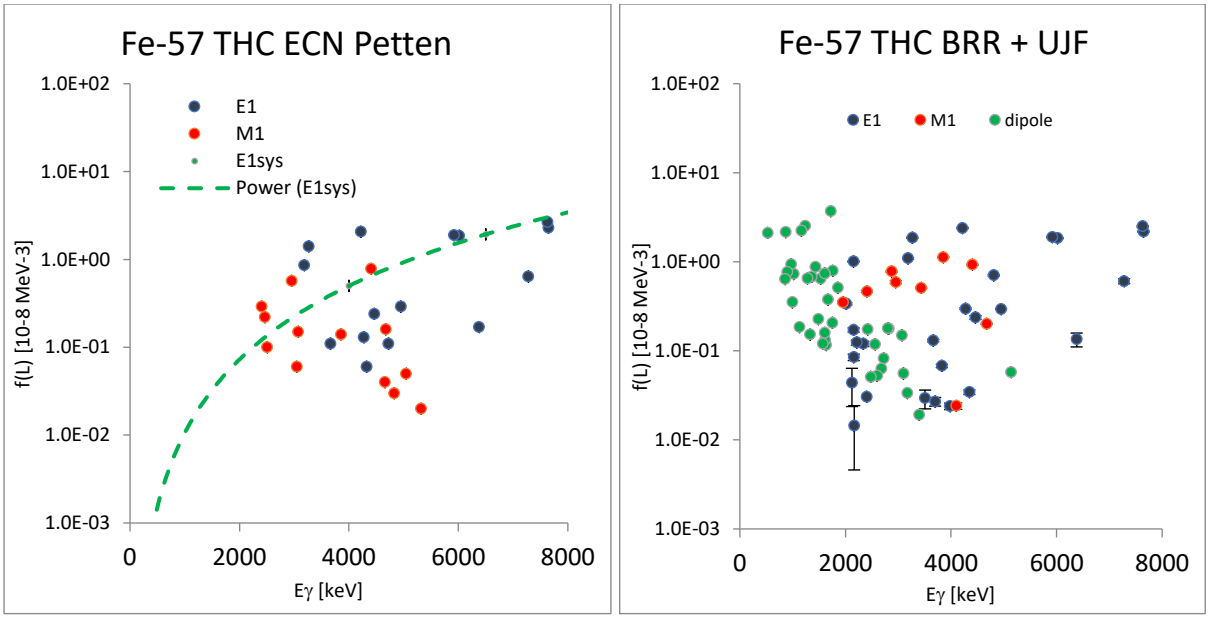

FIG. 1. Left panel: the PSF ^{57}Fe thermal capture data from ECN measurement [6], compared with the <<f(E1)>> 6.5 MeV systematics given by the green dashed line. The E_γ^5 energy dependence is taken from the Brink-Axel parametrization. The E1 data are in a good agreement with the systematic prediction even in the region E_γ = 2-5 MeV. The energy region covered by the data is from 2.4 MeV to 7.6 MeV. The statistical errors are below 10%. Right panel: the recent BRR/UJF data [7] showing many more data points in a much broader energy region from 0.5 to 7.6 MeV and lower sensitivity cut off. The green data points have no ENDSF E_x entries and are at present assumed as dipole radiation. Their primary status has been supported by the coincidence TSC measurements. Note the difference of the active energy region of these two measurements. Three E2 transitions have been included as the dipole entries for the comparison with the OSLO data which assumes all transitions to be of the dipole mode.

The number of assigned primary transitions is influenced by the different low energy cut off between these two measurements, 2.4 MeV and 0.3 MeV respectively. Surprisingly, however, the ΣI_γ (prim) in the energy region ΔE_γ = (2.8 – 7.6) MeV is almost the same, namely 96.6% and 94.4% for the 33 ECN and 41 BRR data entries, respectively. This agreement confirms the quality of the absolute I_γ normalization in both experiments. Furthermore, it indicates that the sum of all 88 primary intensities is ΣI_γ = 98.93(50) % and practically the whole decay strength is included and normalized to the ^{1}H and ^{32}S cross section standards. The 48 low-energy primary BRR transitions between 0.5 to 2.4 MeV have ΣI_γ = 2.3%, most of them with no assigned levels in the ENSDF level scheme and expected to be of dipole nature.

Another important difference between these two measurements is the procedure employed for the construction of the decay scheme. Earlier decay scheme assignments were based on

matching E_γ values and their sums to the adopted level schemes in the ENSDF database [https://www.nndc.bnl.gov/ensdf/], using the Ritz combination principle. Such a procedure was used in the analysis of the ECN data [6] and in many earlier papers with the limitation that when a level is not included in the ENSDF level scheme then such a fit is not a strong argument for the placement of the gammas. However, in the BRR/UJF experiment, the sum γ–γ coincidence method was used to verify the γ branchings and new levels could be identified. This is judged to be a better technique, but it has rarely been applied in such studies till now. The ENSDF literature search has a cut off of 24-sept-1998 and therefore, does not include the new measurements of Ref. [7]. The results of the detailed re-analysis of E_γ, I_γ and PSF data from the $^{56}Fe(n,\gamma)^{57}Fe$ measurements have been submitted to the NDS PSF database.

2.1.2. The direct capture (DC)

The ^{57}Fe nucleus belongs to the group of heavy A < 70 nuclides for which the nonstatistical processes may still compete with an already sizeable statistical compound nucleus CN mode. The direct capture (DC) contribution to E1 transitions in neutron capture has been reviewed in detail in Ref. [8]. There are two empirical methods to verify the presence of the nonstatistical direct component in the thermal capture data. The calculation of partial cross sections for primary transitions, if the (d,p) spectroscopic factor $(2J + 1)S_{dp}$ is known using the Lane-Lynn formalism [10] or from the integral cross-section component σ_{DC} of the thermal cross section σo. Another method is to study the (n,γ)(d,p) correlations between the reduced gamma strength I_γ/E_γ^r and (d,p) $(2J+1)S_{dp}$ factor as a function of the exponent *r* [11].

The contribution of the direct component in the $^{56}Fe(n,\gamma)^{57}Fe$ reaction amounts to 15%, based on the 0.40 b and 2.59 b values for the σ_D and σo, respectively (taken from Refs [8 and 12]). Details of the DC calculation in Ref. [12] are not available, therefore, the DC calculation has been repeated using recent capture data and the results are shown in Table 2.

TABLE 2. Results of the DC calculations using the s(DC) formula from Ref. [12] with f = 9.94 fm and $R = 1.35*A^{1/3}$. The assignments highlighted in yellow are uncertain. The (d,p) spectroscopic factors 'Thom 1974' are taken from J. Thomson NP A227 (1974) 485, 'part.cs' are partial cross sections s_{par} = so*I_g. The total ground state decay of 84% is accounted for.

	Firestone 2017			Thom 1974					
Eγ	Iγ/100n	Ex(nγ)	Jπi	(2J+1)S	Ex(dp)	Jπi		part. cs [b]	**DC [b]**
7646	23.9(4)	0	1/2-	0.287	0	1/2-	23.9	0.61901	**0.0325**
7631	27.1(5)	15	3/2-	1.66	14	3/2-	27.1	0.70189	**0.1869**
7279	5.7(4)	367	3/2-	1.01	367	3/2-	5.7	0.14763	**0.1003**
6380	0.85(15)	1266	1/2-	0.742	1266	1/2-	0.85	0.022015	**0.0515**
6018	9.81(16)	1628	3/2-	0.1	1628	3/2-	9.81	0.254079	**0.0059**
5920	9.6(2)	1726	3/2-	0.176	1726	3/2-	9.6	0.24864	**0.0099**
4275	0.57(1)	3371	3/2-	0.092	3371	3/2-	0.57	0.014763	**0.0019**
4218	4.39(7)	3428	3/2-	0.095	3428	3/2-	4.39	0.113701	**0.0019**
3663	0.16(1)	3983	3/2-	0.088	3974	3/2-	0.16	0.004144	**0.0011**
3267	1.59(3)	4379	(pi=-)	0.130/1.85	4382	1/2+7/2-	1.59	0.041181	**0.0010**
2600	0.020(4)	5046	1/2?	0.022/0.312	5049	1/2+7/2-	0.02	0.000518	**0.0001**
2508	0.030(4)	5138	sec	0.066	5139	1/2-	0.03	0.000777	**0.0002**
							83.72	2.168348	**0.3931**

The resulting value of $\sigma_D = \Sigma\sigma i(DC) = 0.39$ b from the present DC calculation agrees with Ref. [12], which supports the choice of E1 parameters in both calculations and the DC strength is about 15% of the total E1 strength as shown in Fig. 2. Such a DC component is hidden in the PT fluctuations and is included in the systematic error of the trend averaging.

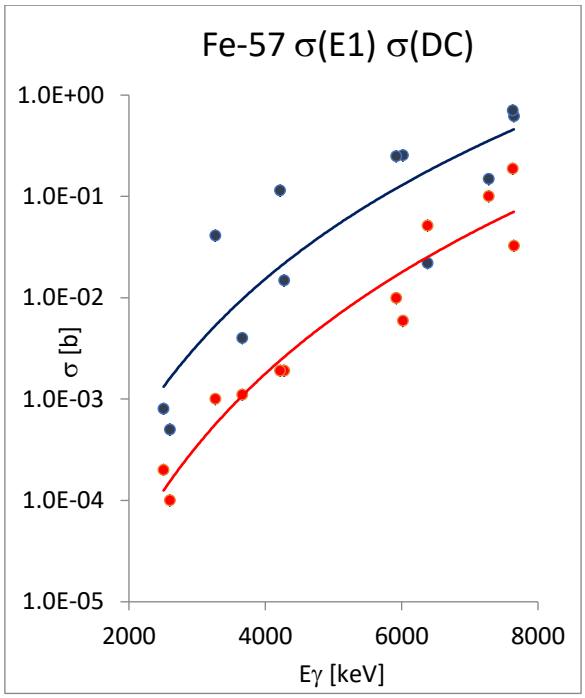

FIG.2. Calculated partial $\sigma_i(DC)$ components compared to partial E1 cross sections. All fitted curves in this work are from the trend line option of Excel, except the theoretical predictions.

The DC contribution of about 15% of the total E1 cross section is supported by the (n.γ)(d,p) correlation analysis shown in Fig. 3 which is, as expected, dominated by strong transitions.

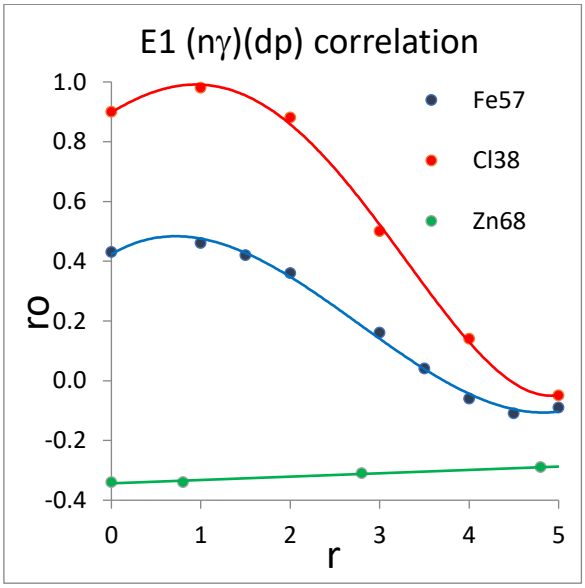

FIG. 3. The $I_{n\gamma}E_\gamma^r$ correlation with the (d,p) $(2J + 1)S_{dp}$ factors. Three nuclides with different DRC components are shown for illustration. From a dominant DRC presence (^{38}Cl) to a medium presence (^{57}Fe) and the fully statistical case (^{68}Zn). The correlation is maximal at r ~ 1 as predicted in Ref. [11].

2.2. Resonance capture

2.2.1. Discrete resonance data (DRC)

The presence of the 2p giant resonance in the light mass region means the DRC data can be used for a comparison of the E1 and M1 modes of the same transition due to the parity switch. The dominant single p-wave resonance is also present in the ^{56}Fe target at E_n = 1.147 keV with J = 1/2- and was measured at the BNL fast chopper in 1970 [9] and included as a data source in the DRC data base. The absolute normalization to a very accurately known 4.9 eV Au resonance is beneficial to compensate some moderate statistical uncertainties.

It is therefore useful to compare these two independent experiments, the thermal and resonance capture, for the absolute intensity calibration. In the THC measurement the calibration from the external calibration sources has been used to derive the absolute intensity in the number of gamma's/100 neutrons while in the DRC measurement the partial radiative widths $\Gamma_{\gamma i}$ has been applied from the time-of-flight measurements. The comparison is shown in Fig. 4 and the similarity between both THC data and the p-wave DRC capture is very satisfactory.

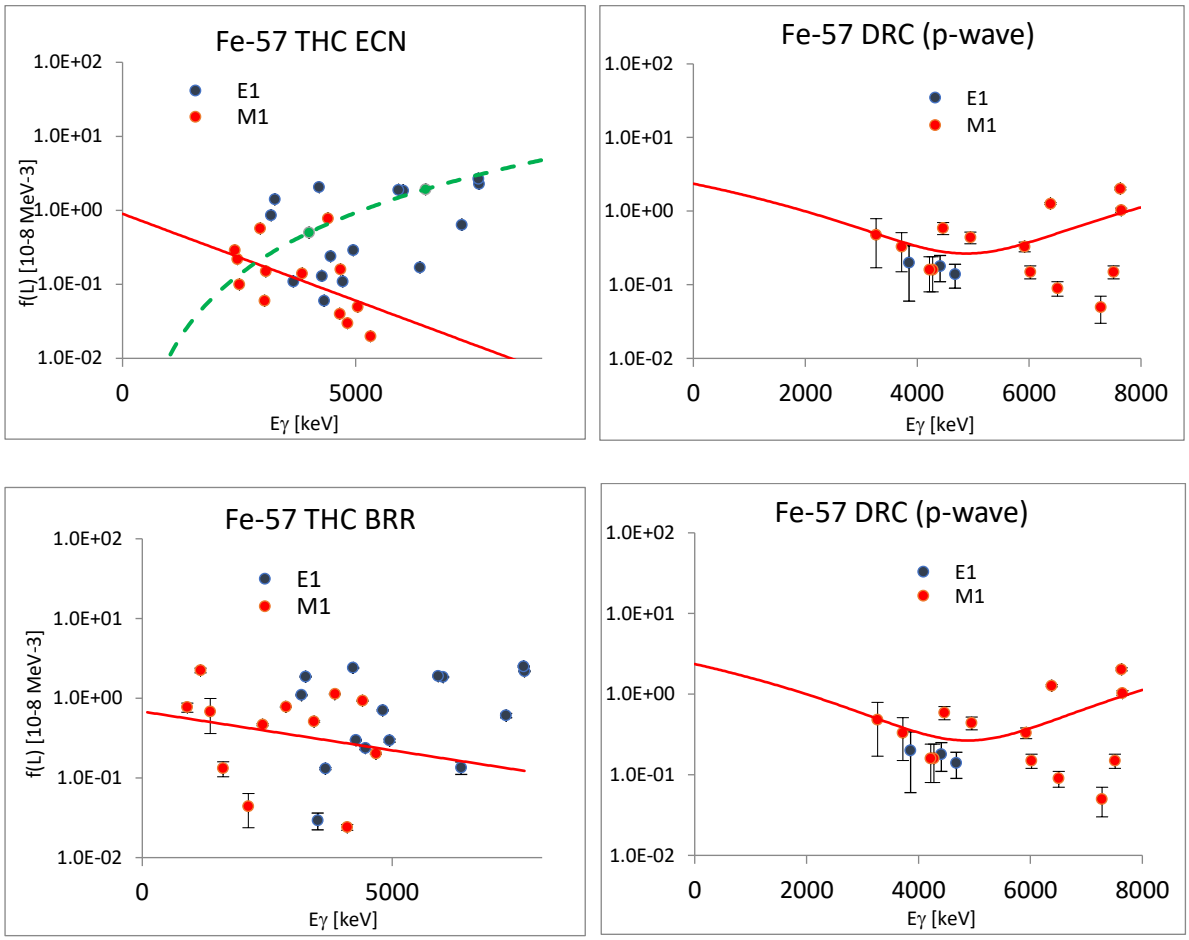

FIG. 4. Comparison of the PSF thermal data ^{57}Fe with the discrete resonance capture from the p-wave resonance at En = 1.147 keV and J = 1/2-. The thermal E1 and M1 data switch their multipolarities in the p-wave capture and are in reasonable agreement with each other taking into account the PT fluctuations. For the DRC PSF analysis the $\Gamma_{\gamma 1}$ and D_1 values from Ref. [12] have been used. Note that there is a certain similarity in high-energy transitions and the increased statistical error of the DRC measurement.

A strong similarity of the high-energy E1 and M1 transition intensities between THC and p-wave DRC data has been noted, later also found in the ^{36}Cl data in Ref. [13] for which a non-statistical influence was suggested. Good agreement of absolute calibrations of these two measurements allows them to be joined in a plot of combined data sets of the ^{57}Fe PSF (THC + DRC) entries as shown in Fig. 5.

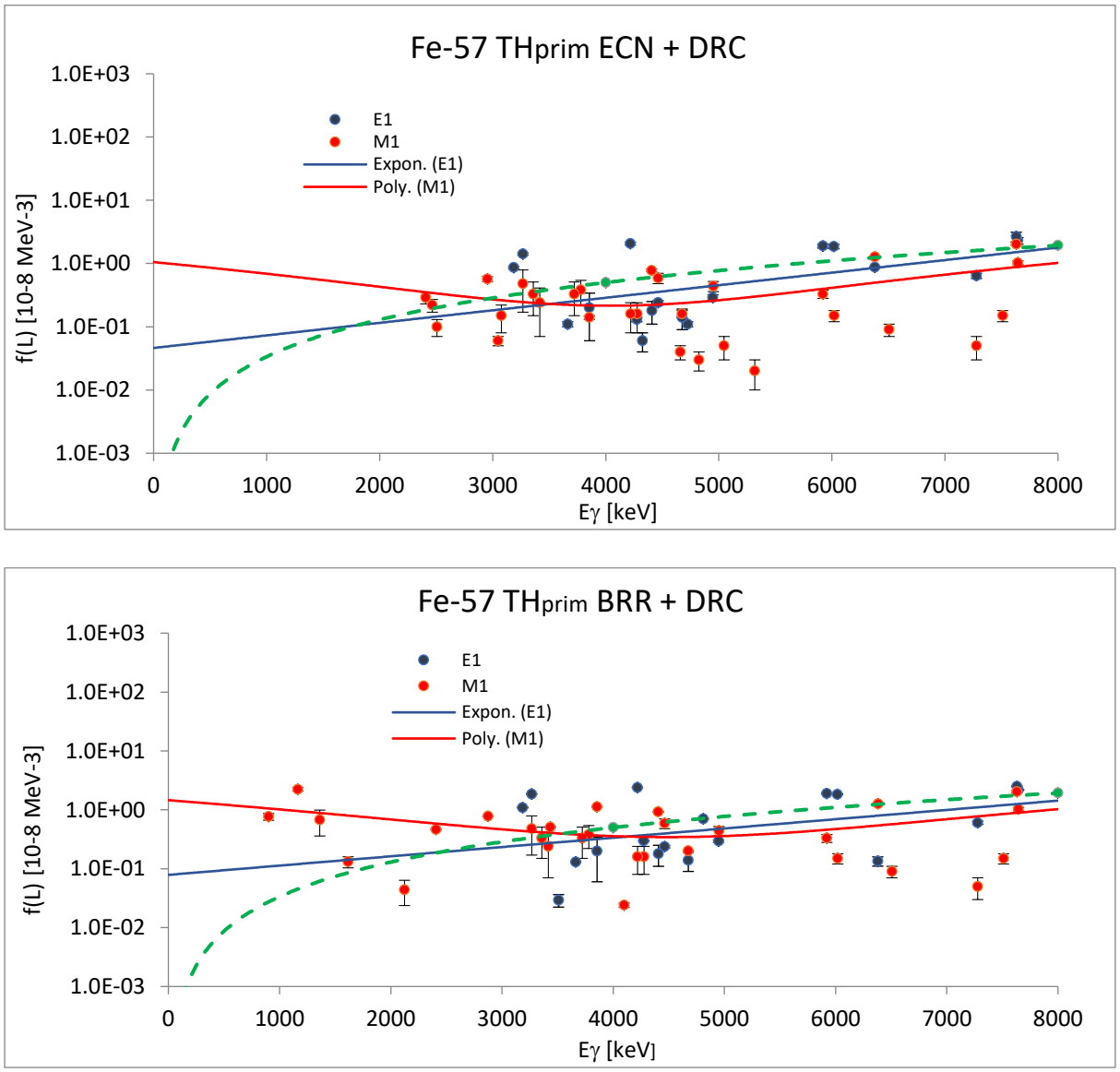

FIG.5. The combined thermal and resonance PSF data of the ^{57}Fe nuclide built from two independent THC experiments and the DRC data. The upper figure uses the THC ECN entries while the lower one shows the recent BRR THC data. Note the good agreement of both E1 and M1 trends towards the zero-energy limit and the agreement of absolute E1 normalizations with the f(E1) systematics (the green dotted curves).

Two observations are worth mentioning. Firstly, the enhanced M1 strength of the high energy data with E_γ > 4 MeV and the data trend projections towards the 0lim region leads to about $0.8*10^{-9}$ MeV^{-3} and $1.5*10^{-8}$ MeV^{-3} for E1 and M1 radiation, respectively. Notably the M1 projection is valid based on primary data down to 1 MeV.

2.2.2. Averaged resonance data (ARC)

The lowest mass of the ARC measurement is the ^{76}As nucleus, the number of resonances in the 2 keV Sc cross-section window below A ~ 70 is too low for sufficient averaging and to distinguish different multipolarities. This averaging is the essence of the gamma-ray strength function definition introduced by Blatt and Weiskopf in 1952 as representing the average electromagnetic property of the nucleus.

This cut off of the ARC data at A ~ 70 increases the importance of the thermal data for the A < 70 mass region as shown in Refs [14, 15]. For heavier targets above A ~ 70 the low E_γ behaviour can be investigated from the ARC data based on the trend analysis [16].

2.3. Comparison with theoretical models

2.3.1. Microscopic and phenomenological models

Thermal capture data have been compared with the D1M+QRPA+0lim (whereafter called D1M+) calculations in Refs [1, 14, 15] as a standard experiment vs. theory verification for the ^{57}Fe ECN data and these are shown in the left panel of Fig. 6. Theoretical predictions agree reasonably well for both E1 and M1 transitions. Note that no primary data have been found below 2 MeV in Ref. [6] contrary to the recent BRR measurement with PSF data down to 0.9 MeV ((Ref [7]) see the right panel of Fig. 6). These have been compared against both models, the microscopic and the empirical SMLO [17, 18]. Only transitions with firm multipolarity assignments have been used for this comparison.

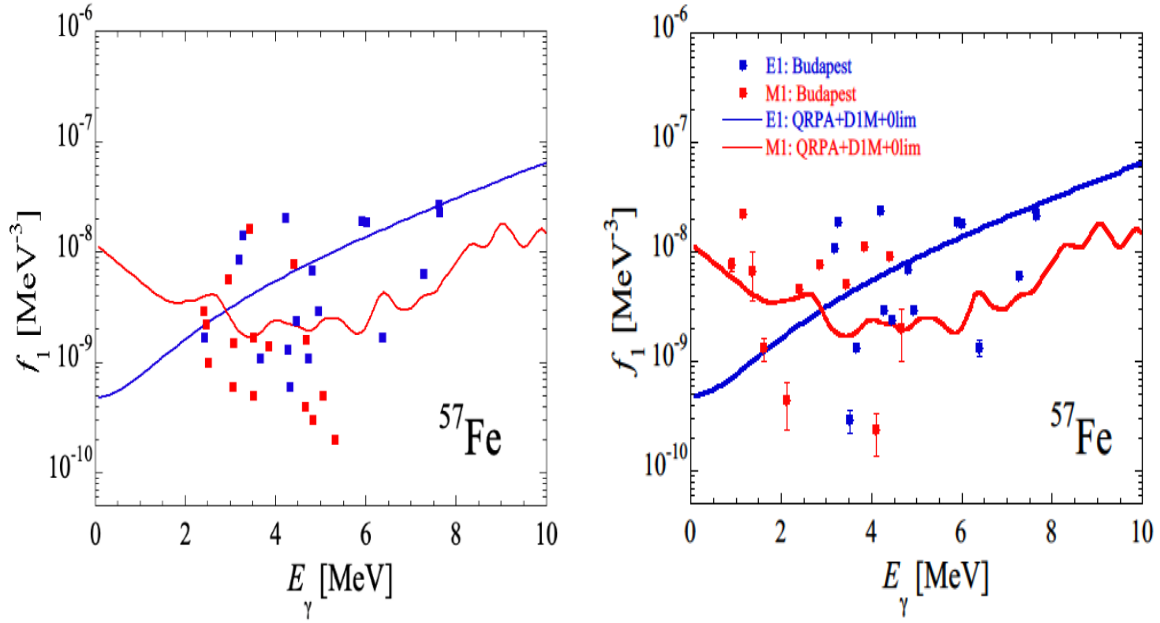

FIG. 6. Left panel shows the comparison n of the PSF ECN [6] evaluation of ^{57}Fe with the theoretical D1M+QRPA+0lim prediction up to 10 MeV. The M1 data are in good agreement with the prediction in the region E_γ = 2 - 5 MeV. The curves show the results of the D1M + QRPA +0lim calculations and the blue and red colors are for E1 and M1 multipolarities, respectively. Note a reasonable agreement between the calculations and E1 or M1 experimental strengths. The right panel includes the recent BRR THC from Ref. [7] and the D1M + QRPA +0lim data again. A general agreement between experiment and theory is maintained.

A visual comparison of the trend zero energy limits in Fig. 6 and the 0lim systematics added to the D1M+QRPA model in Ref. [17] shows reasonable agreement. The adjustment of the free parameters in both systematic equations has been performed and cited in [17] as: *The final E1*

and M1 strengths, including the low-energy contributions and hereafter denoted as D1M+QRPA+0lim can be expressed as the sum of the D1M+QRPA dipole strength at the photon energy ε_γ and the 0lim components E1 and M1 from Eq. 1 and Eq. 2, respectively. The U (in MeV) is the excitation energy of the initial deexciting state of the 0lim exponential component and f0, ε0, C, and η are free parameters. These parameters can be adjusted on shell model (SM) results and available low-energy experimental data such as those obtained with the Oslo method or the average radiative widths and are given in Ref.[17].

These adjustments are such that the low-energy M1 contributions from the 0lim values are around f(M1)~10^{-8} at $E_\gamma = 0$. It was added to the microscopic calculations [17] and the SMLO empirical model [18]. The resulting model predictions are shown in Fig. 7. The E1 radiation agrees also with the older GLO model of Kopecky and Uhl [19]. The parameter adjustments considered Oslo method data in Ref. [17] for $E_\gamma > 1$ MeV data and SM calculations down to the zero limit $E_\gamma < 1$ MeV. Predictions from the ARC trend analysis in Ref. [16] may be included as supporting information for that. However, it must be noted that currently no experimental data are available below 1 MeV. None of the empirical predictions give evidence for a strong low energy enhancement close to the zero excitations.

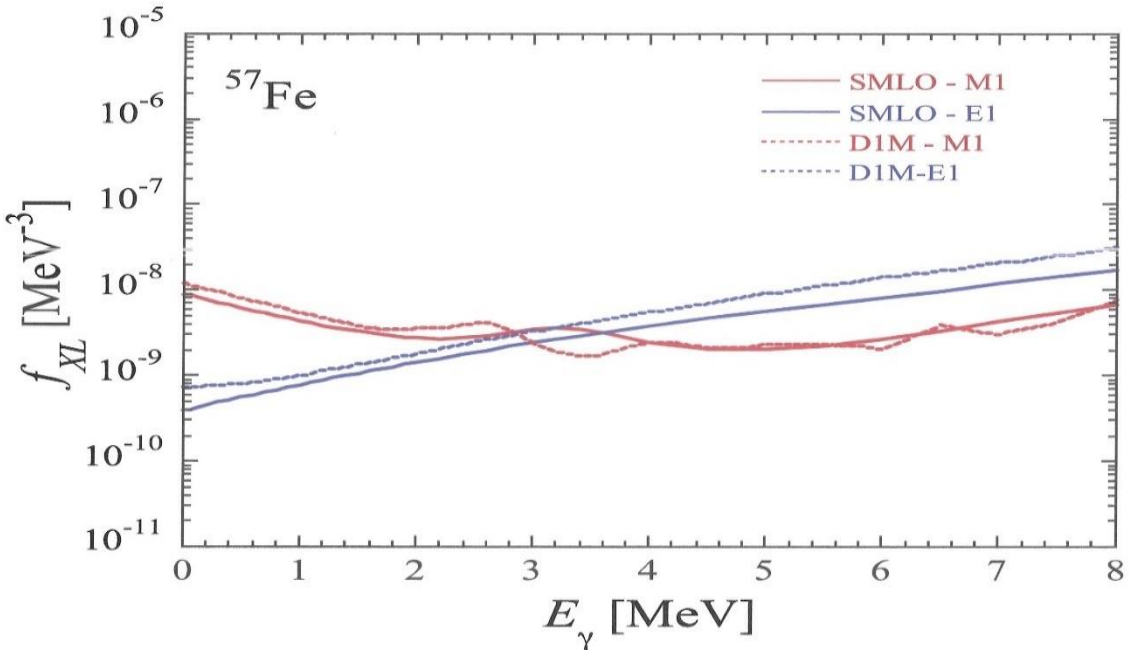

FIG. 7. Recent theoretical predictions of the D1M+QRPA+0lim (dashed curves) and SMLO (curves) models of the ^{57}Fe nucleus (plotted by S.G.).

PSF calculations can be tested by comparing the calculated average total radiative width $\langle\Gamma_\gamma\rangle$ against this integral parameter derived from measured neutron resonances of different s-, p- and d-waves. Two independent $\langle\Gamma_\gamma\rangle$ experimental values for ^{57}Fe obtained from BNL [12] and RIPL-3 sources, $\langle\Gamma\gamma\rangle$ = 0.90(47) eV and 0.92(41) eV, respectively, are in a very good agreement. However, both values suffer from unusually large errors. The calculated values, $\langle\Gamma_\gamma\rangle$ = 1.31eV and 0.79 eV for D1M+ and SMLO models, respectively, were provided via private communication from Goriely with the following comment: *SMLO is directly fitted to photo-absorption data, in contrast to D1M+ QRPA which has been globally adjusted. So, a fine tuning of the PSF might help to improve the D1M+QRPA results.* The combination of theoretical models with the systematics of the low-energy component (0lim) thus enables the comparison

between experiment and theory over the whole energy region and allows for the adjustment of parameters in the zero-limit region (0lim) to be benchmarked against the integral parameter Γ_γ and to test the experimental Γ_γ values. We shall return to this in the last section.

2.3.2. Shell model calculations

The shell model (SM) calculations and their use for the normalization of the 0lim component raise questions because some results give a constant PSF value below 2 MeV [20,21] while some other calculations predict an increasing M1 component with E_γ-> 0 in [22,23]. Especially the SM calculations for the $^{56,\ 57}$Fe isotopes give a dominant strongly increasing low energy M1 component, see Fig. 3 in [22], which disagrees with the present PSF data (see Fig. 5) and also with the 0lim theoretical prediction (see Fig. 7).

2.4. Summary (primary transitions)

The ^{57}Fe PSF data from the thermal and DRC capture (initial E_i energy bin equal to the neutron separation energy or single resonance in the vicinity), are well covered for gamma energies above 1 MeV and are in good agreement with the D1M+QRPA+0lim or SMLO models. The absolute calibration, based on the DRC data systematics, is solidly verified. The behaviour below 1 MeV can be estimated only from the trend analysis. A test of the 0lim systematics over the whole mass range is recommended. It may help in the search for a model for the low energy component.

3. The ^{57}Fe neutron capture secondary transitions

There is a wealth of nuclides, among the THC data with A < 70, where the low-energy transitions have both primary and secondary origin and their extended analysis may bring additional information relevant to on the behavior especially of the M1 components (upbend, scissors mode, spin flip). We have selected the ^{57}Fe nucleus for such a study, because of the firm construction of the decay scheme.

3.1. Selection of secondary transitions

The completeness of the level scheme is an essential pre-requisite for the PSF analysis and must be tested by estimating the quantities ΣI_γ(primary), $\Sigma E_\gamma I_\gamma$/Bn and ΣI_γ (secondary to the ground state) which should be equal and close to one another within their stated uncertainties. The absolute I_γ values, given as I_γ per 100 captures or as the cross section ratio $\sigma_{\gamma i}/\sigma_\gamma$, are tested against fulfillment of the $\Sigma I_\gamma E_\gamma = 100 \cdot B_n$ criterion. Fulfillment of this criterion guarantees that the uncertainty of the absolute normalization is smaller than 10%. These data include not only the primary transitions but also the high-quality secondary transitions, which until now have not been used in the PSF capture data analysis. Several states below B_n have been selected with the following properties: solid assignments in the decay scheme and excellent intensity I_γ (in)/I_γ(out) ratios close to one. These selected states allow the use of their decay as 'primary' bins decay below the neutron binding energy. The selection of these bound states is given in Table 3.

TABLE 3. The ^{57}Fe chosen secondary transitions connect levels with firm spin/parity assignments which guarantees their E1 or M1 determination. The selected initial states of the secondary transitions analysis have been chosen between (1 – 5) MeV and a pilot state 0.705 MeV below 1 MeV. All branching ratios are close to unity, with a medium value of <1.0>. The advantage is that a complete spin/parity environment allows E1 and M1 assignments.

Ei (bin) [keV]	$J\pi_i$	$\Sigma I\gamma in/\Sigma I\gamma out$	$\Sigma in/\Sigma out$	Ex [keV]	$J\pi_f$	$E\gamma$ sec
4692	5/2+	0.38/0.33	1.15	136	5/2-	4555
				1725	3/2-	2967
				2207	5/2-	2485
				2505	5/2+	2187
				2971	3/2-	1721
4210	3/2-	2.07/2.01	1.03	0	½-	4210
				14	3/2-	4195
				136	5/2-	4073
				367	3/2-	3842
				707	5/2-	3503
				1265	½-	2945
				1628	3/2-	2582
				2118	5/2-	2092
				2208	5/2-	2002
				2505	5/2+	1705
				2575	(3/2)-	1635
				2921	½-3/2-	1289
				2971	3/2-	1239
				3298	½+3/2+	912
3240	½-	1.97/2.03	0.97	0	½-	3240
				14	3/2-	3226
				136	5/2-	3103
				1266	3/2-	1974
				1726	3/2-	1514
				2208	5/2-	1032
				2505	5/2+	735
				2574	3/2-	666
2836	3/2(+)	2.09/2.26	0.93	0	½-	2836
				136	5/2-	2700
				367	3/2-	2469
				706	5/2-	2129
				1628	3/2-	1209
				1725	3/2-	1111
				2118	5/2-	2118
1725	3/2-	10.99/11.05	0.99	0	½-	1725
				14	3/2-	1711
				136	5/2-	1589
				367	3/2-	1359
				706	5/2-	1019
				1625	½-	460
706	5/2-	6.89/7.07	0.07	0	½-	706
				14	3/2-	692
				136	5/2-	570
mean<value>			<1.0>			

We have tested these two data sets (primary and secondary transitions) from the ^{57}Fe BRR data and the reduced transition intensities I_γ/E_γ^3 are shown in Fig. 8. The difference between primary transition intensities, with $E_\gamma < 2$ MeV from states with $E_i \sim B_n$ to $B_n - 2$ MeV, and the secondary ones with the same $E_\gamma < 2$ MeV energy from states below Ei ~ 4 MeV to the ground state, is evident. The reason may be partially due to the different transition mechanisms. This observation influences the choice of experiments using initial states below the neutron separation energy (bound states in the neutron capture terminology) for the γ-strength decay and consequently the PSF values. The primary transitions below 1 MeV are assumed to be even dipole transitions, while the secondary transitions are firmly assigned (all spins known) as the dipole transitions with E1 or M1 multipolarities.

The ratio of the mean $\langle I_\gamma/E_\gamma^3 \rangle$ strength of secondary and primary transitions below 1 MeV is about ~ 30, based on 12 and 6 secondary/primary transitions, respectively. The low energy intensity enhancement of the secondary transitions had already been noticed in the early sixties. This excess is partially due to the strength transfer from high energy states, populated by primary transitions, to the ground state to satisfy the out/in condition of the capture and ground states. This may bring an unexpected problem for the PSF dependence on the initial state energy if different experimental methods with different initial excitation energies are exploited for the final nucleus excitation.

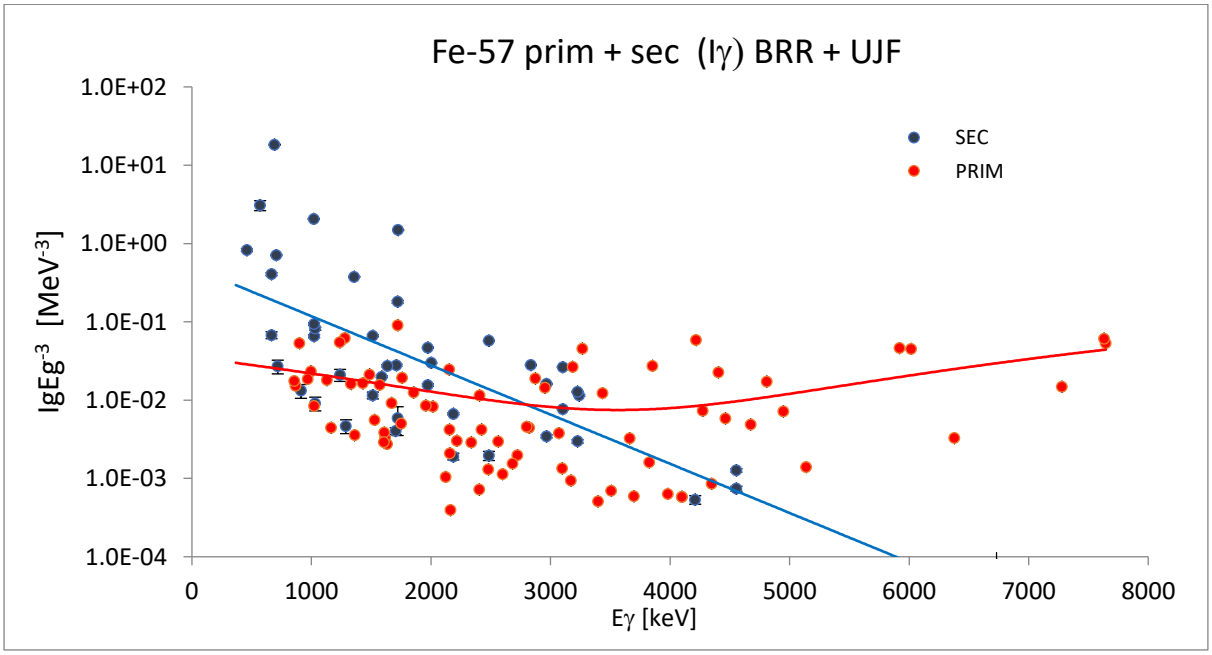

FIG. 8. The combined primary and secondary data from different initial states from Ref. [7]. The B_n capture state and six bound levels at E_i = 750, 1725, 2836, 3240, 4210 and 4692 keV have been used. Note the smooth overlap of both data sets between 2- 4 MeV and the increase of the secondary strength below 2 MeV. The plotted curves serve as a trend of the E_γ dependence. The plotted data are in absolute I_γ/100 neutron captures/MeV^{-3} scale without multiplication by the radiative width $\langle \Gamma_\gamma \rangle$.

3.2. Conversion to the PSF values

The use of the secondary transitions in the PSF analysis requires a conversion of the reduced I_γ/E_γ^3 intensities into the PSF format. An empirical way to deduce the bound state width Γ_γ (from the known half-lives of bound states) and the level spacing D_x (from the cumulative plot of discrete levels) has been chosen. The empirical results for ^{57}Fe are shown in Figs 9 and 10.

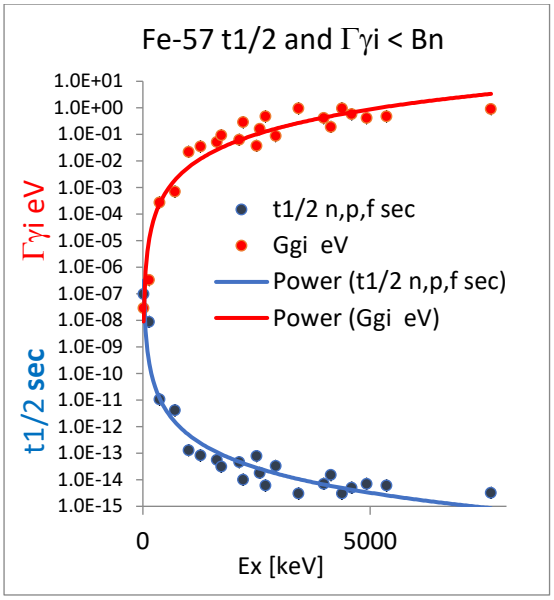

FIG. 9. Plot of the bound state $t_{1/2}$ and $\Gamma\gamma_i$ parameters for the ^{57}Fe nucleus as a function of excitation energy in ^{57}Fe. Only states with J=1/2, 3/2 and 5/2 spins have been considered because of the dipole dominance of transitions. The thermal capture-state half-life has been extracted from the $\langle\Gamma\gamma\rangle$ = 0.9 eV value from the resonance region. Note the dramatic change of both parameters in the Ex < 1.5 MeV region.

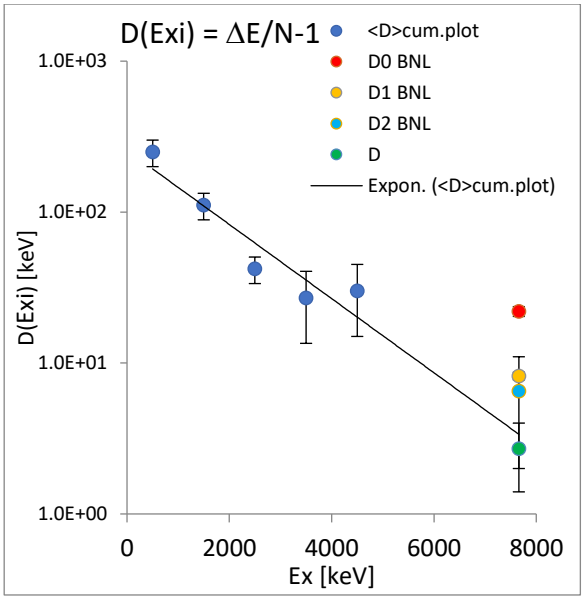

FIG. 10. The average spacing below 5 MeV was extracted from the ENDSF cumulative discrete levels plot for bins one MeV broad. The first three lower data points below 3.5 MeV include all states from the decay scheme. The two remaining points start to miss states and the uncertainty is therefore increased to 50%. Spins outside the ½, 3/2 and 5/2 configurations have been neglected, expecting minor contributions. The data at 7.6 MeV belong to the neutron separation energy and have been extracted from Ref. [12] (see further). Note the spread of spacings below the D0.

The ^{56}Fe resonance data include 42 s-, 123 p- and 124 d-resonances, respectively, with energies up to 0.85 MeV above the neutron separation energy S_n. For the s- and p- resonances the D_0 and D_1 spacings are given in Ref. [12] and the remaining D_2 and total spacing D have been estimated from the list of resonances in this work.

The combined PSF data from secondary and primary transitions, using the estimated level densities at the three E_i bins using capture states below 5 MeV and 7.6 MeV, are shown for both (n,γ) experiments [6, 7] in Fig. 11. The empirical approach to identify the $\langle\Gamma_\gamma\rangle$ and D values from Figs 9 and 10 have been used to obtain an indication of the PSF data behaviour, in particular possible secondary non-statistical transitions. Results shown in Fig. 11 indicate that there is a gross agreement between the primary and secondary data taking into account the uncertainties of the input parameters together with PT fluctuations. For this reason, a plot with 1 MeV broad PSF bins from [7] is added in Fig. 12. The absolute uncertainty of all PSF data stems from the uncertainty of the average radiative widths $\langle\Gamma_\gamma\rangle$ = 0.90(47) eV from BNL. This uncertainty, however, can be reduced by means of the DRC f(E1) systematics, because of the partial resonance Γ_γ used in this analysis, which is in excellent agreement with the D1M+QRPA prediction at 6.5 MeV as a function of the mass [24].

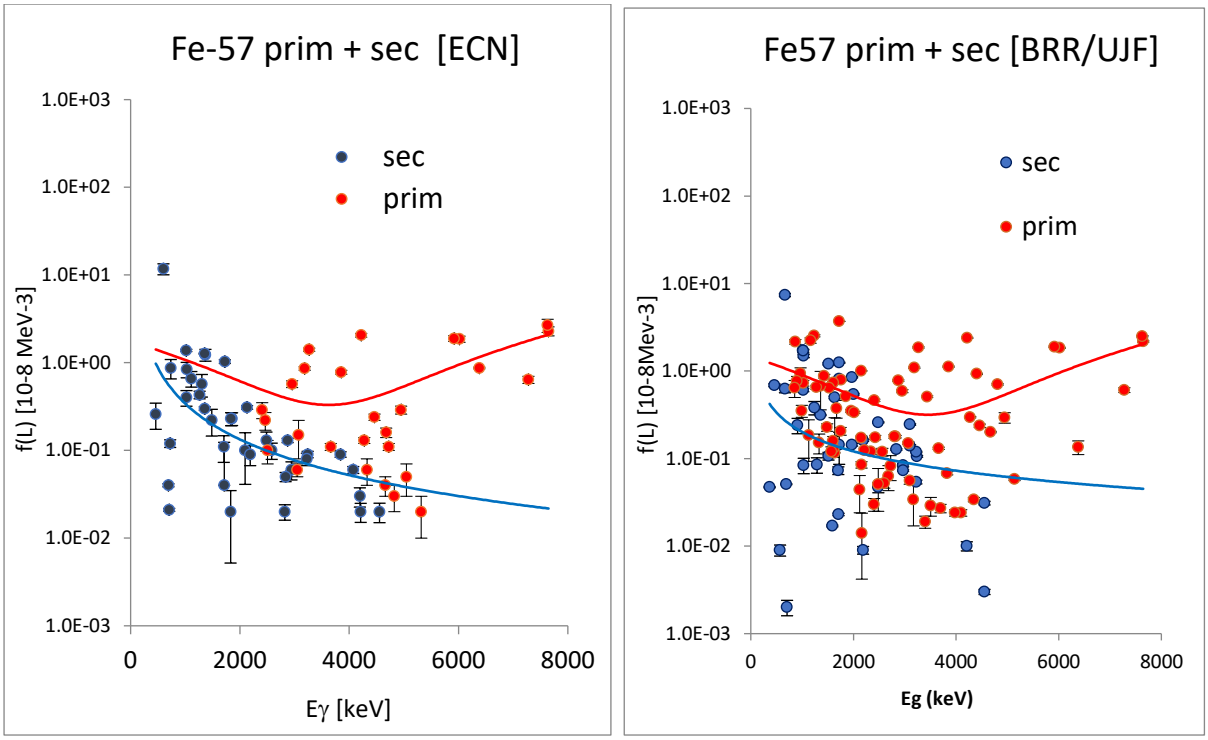

FIG. 11. The combined primary and secondary PSF data from different initial states using Refs [6, 7] capture data. The plotted red curve reflects the expected shape of the PSF energy dependence from the E_i = 7.6 MeV B_n state shown as a polynomial dependence of the statistical and low energy 0lim components. Note that the PSF data trend of secondary transitions (blue curve), using bound states populated within the (n,γ) decay, reasonably agree with that expected from primary transitions close to the zero energy. No strong enhancement has been observed. This may be one of the distinctions with the charged particle method populating a much broader spin region.

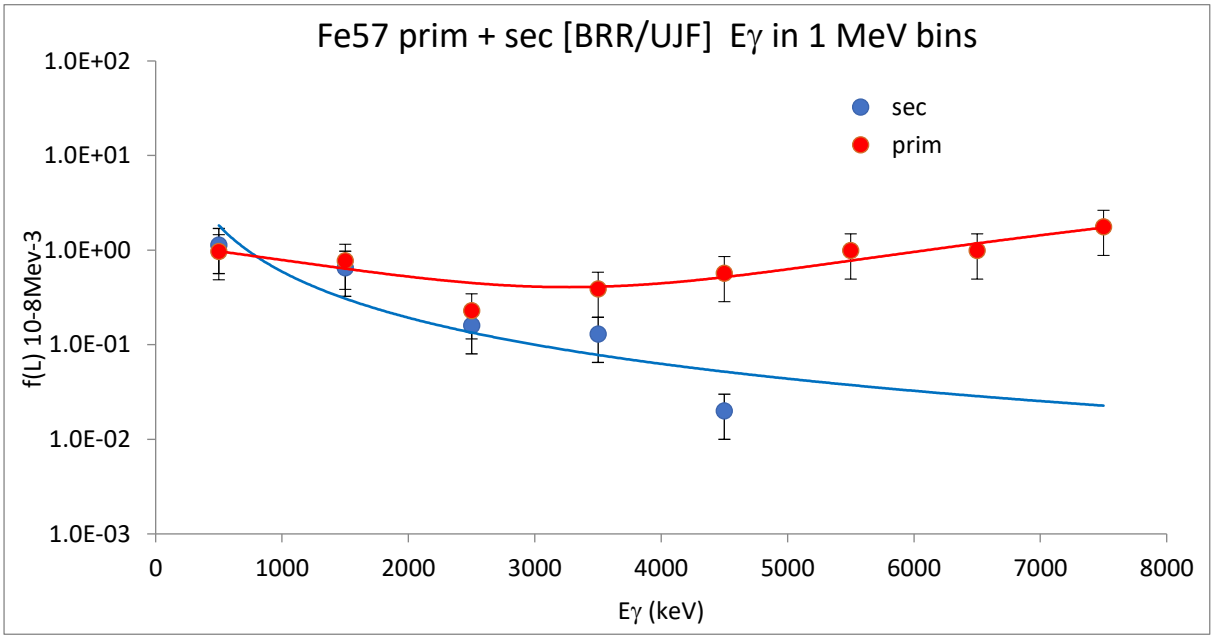

FIG. 12. The combined primary and secondary PSF data from different initial states using Ref. [7] capture data. The B_n energy and three level density bins of states in E_i = 0 -1 MeV, 1-3 MeV and 3 - 5 MeV windows, extracted from Fig. 10 data, have been used. Note the 0lim value of about 10^{-8} MeV^{-3} at zero energy displaying no enhancement with respect to the values expected from the trend analysis in neutron capture [16].

Summary (secondary transitions)

There are several weaknesses in this analysis, such as the use of the half-life values from the estimated trend fit for a state without measured data or the use of the cumulative discrete levels plot for the level density estimate. Figure 12 includes all states below 3 MeV and states with spins beyond the dipole transitions reach. This uncertainty may bring an underestimation in the derived spacing. However, we believe that the adopted uncertainty of about 50% is a reasonable guess and this pilot procedure gives relevant information from analyzing the experimental data using the initial states below the neutron separation energy. The main source of the uncertainty comes from the secondary transitions, which with decreasing E_γ and energy of the initial bound states (see Fig. 8) may not originate from the quasi-continuum as expected for statistical observables.

The use of secondary transitions isn't meant to supplement the PSF data from primary transitions. Instead, the goal was to generate PSF data from excitation Ei bins in the bound state region to simulate the Oslo method and compare the results with Oslo data.

4. Comparison with other ^{57}Fe data

As mentioned in the Introduction, four PSF measurements have been published for the ^{57}Fe nucleus using charged-particle reactions for the ^{57}Fe nucleus excitation, two measured with the Oslo method [2, 3] and, recently, the two (p,p') experiments [4, 5]. Notably Ref. [2] was the first time a low-energy enhancement was observed: *"we report on the first observation of a strong enhancement of the soft PSF in ^{56,57}Fe over the model predictions*".

The Oslo method consists of a combination of a rather complex experiment and data analysis that has been discussed in many explanatory and or critical publications [24-26]. We compare the results obtained with the Oslo method with the neutron capture data and try to quantify the differences between these two methods.

In Fig. 13 we present the Oslo data from Ref. [2] and show how this data developed from 2004 until the submission of data to the IAEA PSF database in 2018. As a first observation, the absolute calibration performed in 2004 has been revised because the (3–7.6 MeV) bin in the right-hand plot is more than a factor of two weaker. The PSF absolute scale is, according to the text in the database Readme file, normalized to the average Γ_γ of neutron resonances which has an estimated 24% error, including the violation of the equal amounts of positive/negative parity states below S_n. Therefore, the absolute normalization of the Oslo measurements seems rather questionable which in turn calls into doubt the PSF data in the low energy region. See also a general description of the Oslo method uncertainties in Ref. [25]. Especially the absolute normalization of the transmission coefficient to $<\Gamma_\gamma>$ may be the source of uncertainty as shown in Ref. [27], where an error in the normalization code of 30% was discovered in 2014, probably also present in all the data published before. Kopecky [28] compared the (n,γ) and Oslo PSF data from the IAEA 2019 PSF database and encountered several disagreements.

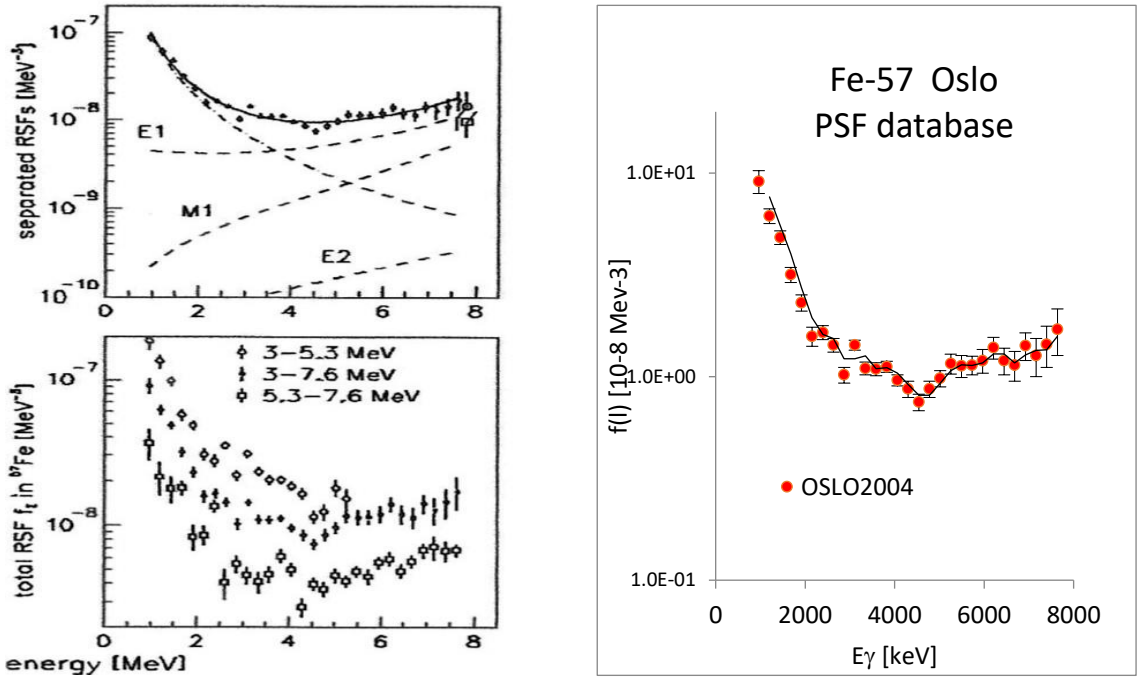

FIG. 13. The PSF ^{57}Fe values extracted from the original Oslo 2004 publication [2] in the left panel taken from Ref. [2]. In the left upper panel, the decomposition of theoretical models and the proposed power law energy component are shown. Note the difference between the lower data in the (3-7.6 MeV) window and the final data (solid curve) in the upper part. Further note in the lower part the influence of different excitation energy windows on the PSF magnitude. In the right panel are the same 2004 data taken from the IAEA PSF database released in 2019.

Interesting is the lower plot in the left panel which displays the influence of the initial state energy (window or bin) on the magnitude of the average strength function. This effect shows that the closer the window is to the S_n energy the closer the PSF magnitude will be to values from neutron capture. Also notable is the similarity between the secondary transitions approach and Oslo measurements using the bound levels < B_n as the initial states of the gamma decay.

Detailed comments on the TSC validation of the PSF enhancement are outside the scope of this report but note the missing discussion of the typical uncertainties for low-energy gamma rays like the crosstalk effects in coincidence measurements, predicted in the GEANT3 calculations by Rusev in Ref. [29].

For comparison, the thermal data have been converted into the dipole mode respecting this Oslo assumption that what is extracted is total dipole strength. However, several firmly assigned E2 data points show that the strongest E2 data may in the E_γ^3 reduction appear as M1 data. Fig. 14 shows the binned neutron capture BRR data from Ref. [7] in the left panel while in the right panel they are compared with the older ECN data.

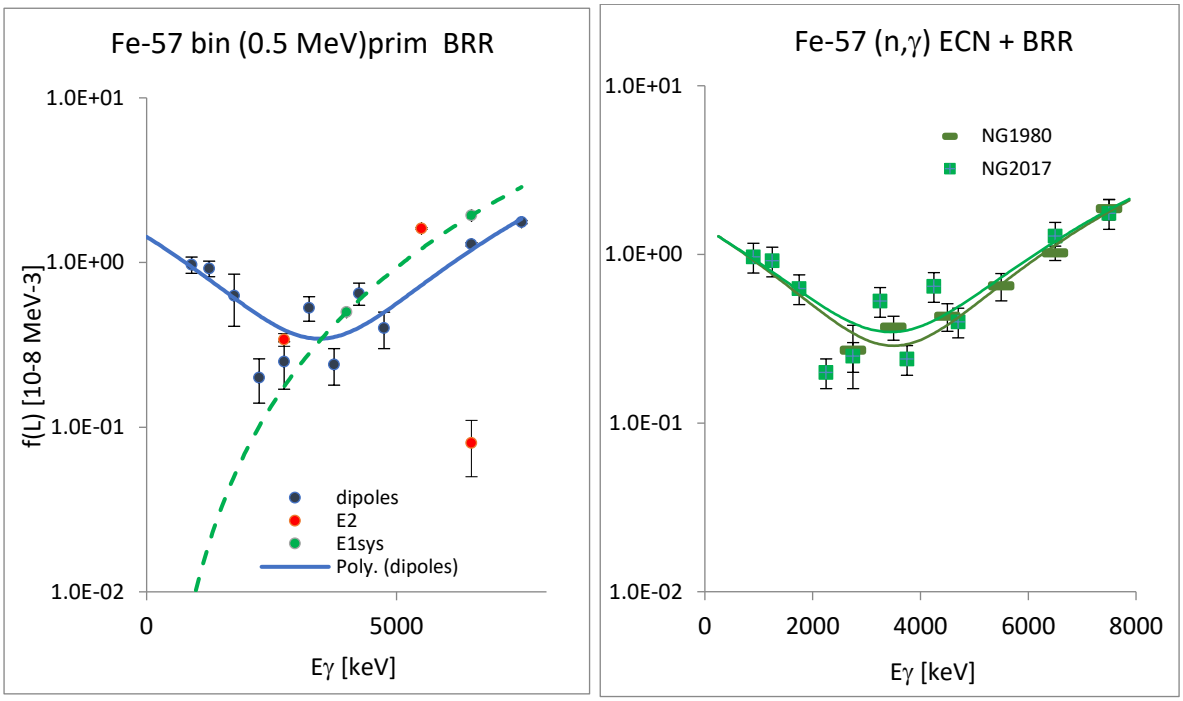

FIG. 14. The binned (0.5 MeV bins) BRR primary transitions, shown in the left panel, including three assigned E2 transitions, all used intensities are the I_γ/E_γ^3 reductions. The green dashed curve stems from the average <PSF (E1)> systematics. The good agreement between ECN (1980) and BRR (2017) binned data is shown in the right panel, confirming the quality of the absolute normalization and agreement of dominating transition strength.

These data are compared with the two ^{57}Fe(^{3}He, ^{3}He')^{57}Fe Oslo measurements in Fig. 15. The Oslo data have been taken from the present IAEA PSF database. The shape of the 2008 data looks similar to the (n,γ) curve, only the absolute magnitude is about 2 - 3 times higher. This difference can easily be understood by the systematic uncertainties, especially those affecting the Oslo data.

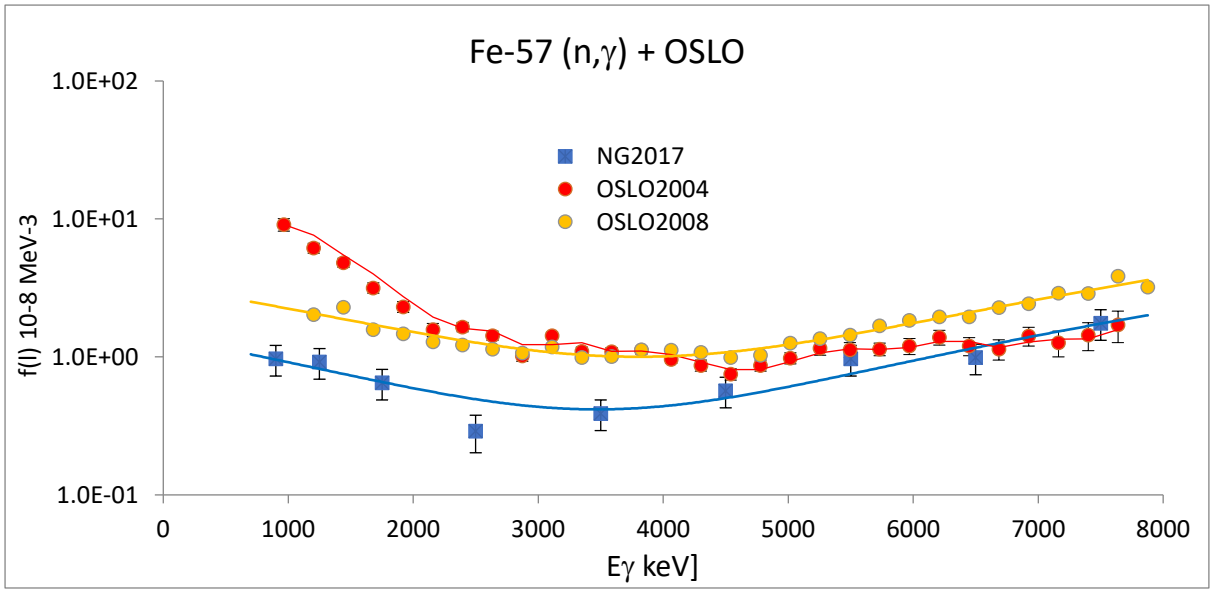

FIG. 15. Comparison of the PSF dipole data from the primary BRR neutron capture data points (blue) with the Oslo data [2,3]. All fitted curves are either polynomial or moving average functions. Note the rather small uncertainties for charged-particle reactions and the significant difference between the Oslo 2004 and 2008 measurements below 2 MeV as well as between the Oslo and the capture data.

The ^{56}Fe data have been measured with the (p,p') reaction. It is interesting to compare these results with the ^{57}Fe data given the similarity of the PSF data of both isotopes, as shown in Refs [2, 3] and Fig. 16.

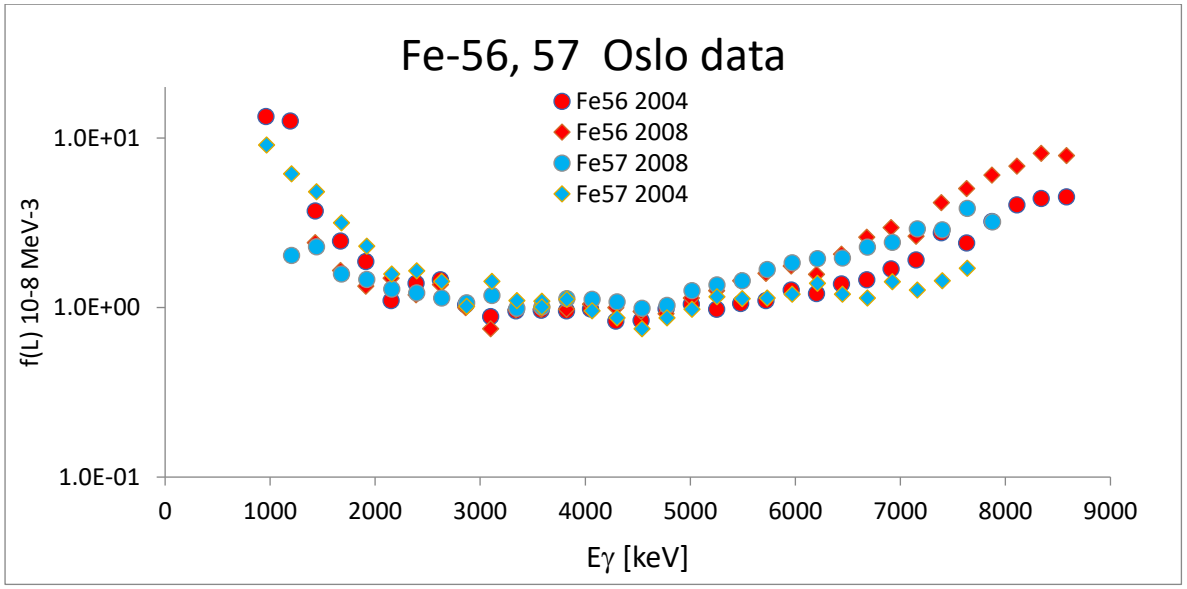

FIG. 16. Displayed are PSF data from Oslo experiments with the enriched ^{57}Fe isotope using the ^{57}Fe(^{3}He, ^{3}He')^{57}Fe and ^{57}Fe(^{3}He,αγ)^{56}Fe reactions. Note the similarity of the data of the two neighboring product nuclides (red and blue data points for ^{56}Fe and ^{57} Fe, respectively). This feature allows us to include both the ^{56}Fe and ^{57}Fe measurements in the intercomparison.

This similarity allows us to compare PSF data from the ^{3}He-induced reaction on ^{56}Fe with the two ^{56}Fe(p,p') measurements as shown in Fig. 17.

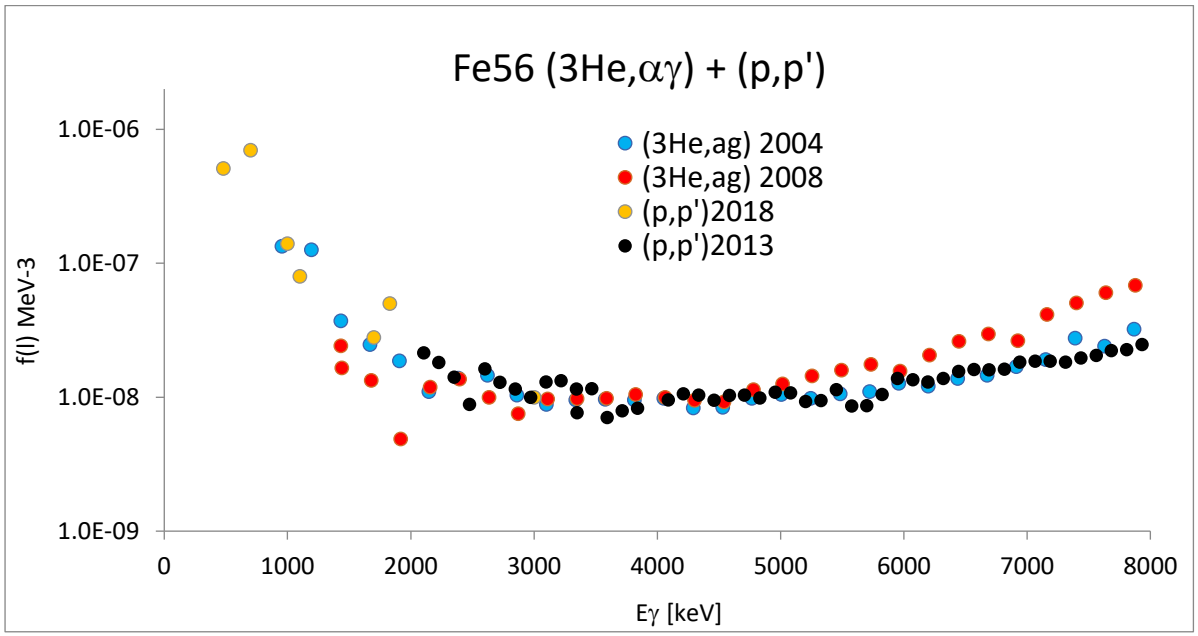

FIG. 17. The Oslo and (p,p') 2013 [4] data have been taken from the present IAEA PSF database but the latest (p,p') ratio method data [5] have not yet been included there. These latter data have been extracted from Fig. 2 of Ref. [5] and set equal to data from Ref. [4] at 3 MeV. Note the sharply increasing strength below 1 MeV from the ratio method and that only two measurements provide data below 1.5 MeV. The polynomial trend fit has been used only in the $\langle\Gamma_\gamma\rangle$ calculation test (see further).

The PSF data from Refs [2, 3, 4] are "integral" data using all initial energy bins, while the latest (p,p') results are shown partially in five 0.5 MeV wide bins from E_x = 3.5 to 7.5 MeV. The effect of increasing PSF strength with decreasing bin energy is shown in Fig. 2 of Ref. [5] and shows the PSF strength dependence on the initial excitation energy.

Summary (comparison with other data)

There is obviously a strong disagreement between the (n,γ) and both Oslo and (p,p') PSF results., One reason may be the different initial excitation energies. While the neutron capture uses resonance states above the threshold energy with almost constant level density with quasi-monoenergetic excitations E_i, the charged-particle reactions preferentially populate states below the neutron capture threshold with rather different initial energies, spins and parities.

The enhanced low-energy (LEE) components from the bound state excitations should be considered as not fully compatible and may impact any subsequently derived quantity such as the average radiative width $<\Gamma_\gamma>$, gamma-ray spectra or cross sections at energies close or above the neutron threshold (see Sec. 1.3). This was tested here by calculating the $<\Gamma_\gamma>$ value using the D1M + QRPA with the 0lim component equal to the 2004 Oslo data (blue curve in Fig. 17). The result of this calculation [31] was $<\Gamma_\gamma>_{cal}$ ~ 2.7 eV which is about three times larger than the BNL Atlas value [12] and raises the question of the transition coefficient normalization used in Ref. [2].

5. Conclusions

Two independent neutron capture experiments have been carefully compared and shown to have very good agreement. This confirms that the neutron capture method is a solid experimental, model-independent tool with well understood data analysis. The capture PSF data presented for ^{57}Fe, describe data above Eγ ~ 0.5 MeV for E1, M1 and E2 radiation. This data has been included in the updated IAEA PSF database.

The absolute normalization has been verified from theoretical predictions based on the D1M + QRPA model in Refs [15, 24] and forms a firm calibration standard for the E1 high energy statistical component (see Fig. 18). The D1M+QRPA entries are based on individual 6.5 MeV bin calculations for the same nuclides as the experimental input. The recommended f(E1) formula $<f(E1)> = 0.0042\ A^{(1.7 \pm 0.3)}$ for the <6.5(5)> MeV energy bin in Ref. [24] nicely reflects the f(E1) mass dependence. This normalization was applied in previous neutron capture DRC and ARC studies and has been used in this work for comparison.

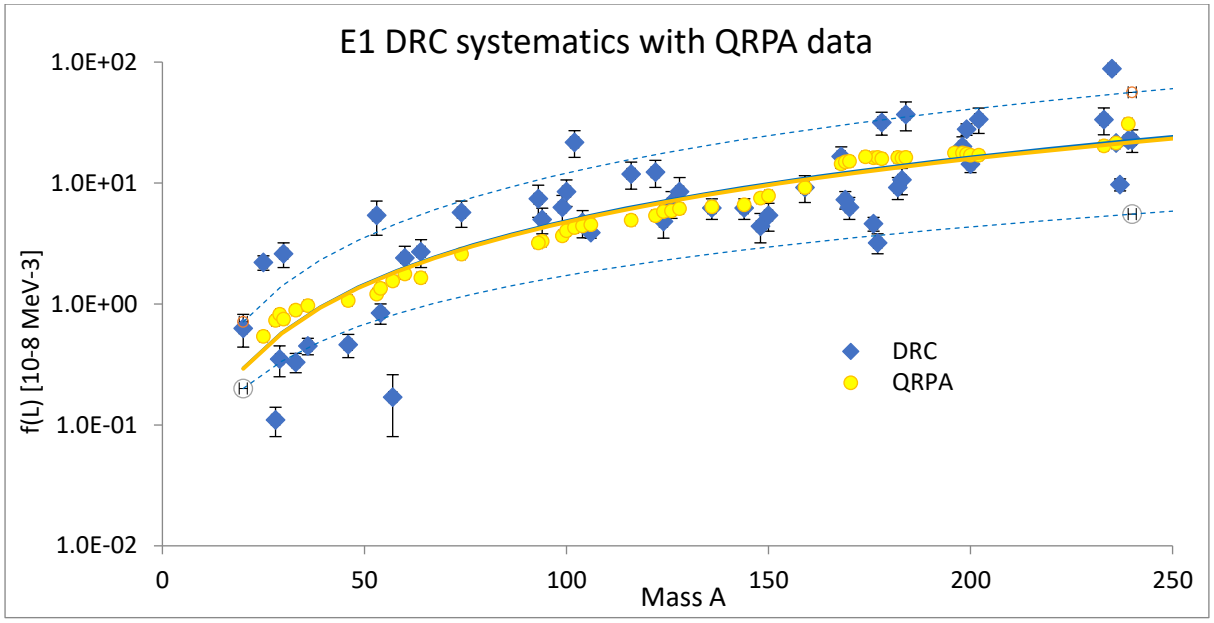

FIG. 18. Quasi-mono energetic doubly averaged DRC strength functions <<f(E1)>> compared with the microscopic D1M+QRPA predictions over the 6.5 ± 0.5 MeV region. Note the excellent agreement between both fitted trend curves andher the (n,γ) data. Details of the outliers are discussed in Ref. [24].

However, the disagreement of PSF data from charged particle and capture data below 2 MeV is striking. The low energy Oslo data of Voinov [2] for ^{57}Fe are also in significant disagreement with the data of Algin et al. [3]. No explanation of this difference is given which probably reflects problems in normalization of both level density data and the transmission coefficients.

Despite the improved low-energy transition sensitivity of the Budapest experiment (the lowest transition of 368 keV) the number of TSC verified primary data below 1 MeV is limited. To be specific, only seven transitions between 368 and 995 keV have been assigned in Ref. [7] as primary transitions, six of them without multipolarity assignments and only one transition was assigned as a M1 using a weak argument. For completeness, no data below 1 MeV have been reported in any Oslo measurements, except for two data points in the ^{56}Fe(p,p') measurements (at ~ 0.7 and 1.0 MeV). This implies that a direct experimental confirmation of the low-energy enhancement effect below 1 MeV in ^{56,57}Fe nuclides is missing and that current claims are based only on the trend predictions. This trend strongly exceeds the low energy capture data (see Figs.14-16). Attempts to find such data from statistical model simulations have been disregarded.

Magnitude disagreements between the capture and charged-particle induced data can also be influenced by different initial energies in experiments with various initial level densities. The Blatt and Weiskopf definition says that PSF represents the average electromagnetic properties of a nucleus which is model independent and depends only on the energy E_γ. However, this independence is valid only for the level density or spacing D used in the particular experiment together with a full validity of the Brink hypothesis. This is true in capture experiments with initial states close to the neutron separation energy, including the thermal capture state or narrow quasi-continuum discrete resonance region with about equal level density parametrization. In such a case the PSF value is dependent only on the energy E_γ and its partial

intensity $I_{\gamma i}$. One consequence is that the PSF values from experiments with different initial energies become incompatible with capture data.

Any physical modelling describing the low-energy enhancement, especially for the M1 radiation, will be a big step forward to a better understanding of the PSF behavior below 2 MeV. For E1 the direct capture in light mass nuclides is available, but no similar formula is applicable for the M1 formalism. The reduced I_γ (M1) correlation with (2J + 1) S_{dp} factors was found for a few nuclides in the 2p – 3s orbitals region and interpreted by a semi-direct mechanism [30]. An M1 nonstatistical signature was found in p-wave resonance capture measurements on ^{36}Cl and ^{57}Fe nuclides [9,13] with a strong correlation between s-thermal and p-resonance E1 and M1 intensities.

Summary of Conclusions

The neutron capture PSF data disagree with all low energy ($E\gamma < 1.5$ MeV) data from the Oslo and (p,p') experiments and predict a much smaller enhancement effect. The (n,γ) results are in agreement with the E1 GLO model [19] and the E1 and M1 0lim predictions from theoretical models [17,18].

The gamma-ray strength function describes the γ-decay properties of a nucleus at high excitation energies with related level densities and represents the average (over the initial excitation) reduced γ-ray transition probability for the given transition energy E_γ and multipolarity L from the initial excitation E_i, thus $f(L) \sim f(E_\gamma,E_i)$. Lower excitation energies below the neutron separation energy include several effects which may influence the PSF behaviour.

Acknowledgement

JK gratefully acknowledges the IAEA NDS for initiating and supporting his work in recent years and particularly the interaction with and help of Vivian Dimitriou. The continued supervision by and advice from Stephane Goriely have been very valuable. Discussions with M. Krticka and S. Valenta are acknowledged as well as with R. Forrest. This would not have been possible without the overarching support of the Nuclear Data Section Head, Arjan Koning.

References

[1] S. Goriely, et al., Eur. Phys. J. A **55** (2019) 172.
[2] A. Voinov, et al., Phys. Rev. Lett. **93** (2004) 142504.
[3] M. Algin, et al., Phys. Rev. C**78** (2008) 054321.
[4] A.C. Larsen, et al., Phys. Rev. Letters **111** (2013) 242504.
[5] M.D. Jones, et al., Phys. Rev. C**97** (2018) 02432.
[6] R. Vennink, et al., Nucl. Phys. A**344** (1980) 421.
[7] R. Firestone, et al., Phys. Rev. C**95** (2017) 014328.
[8] J. Kopecky and F. Becvar, Thermal Neutron capture in the Low Mass Region, IAEA report INDC(NDS)- 0886, 2023, https://www-nds.iaea.org/publications/indc/indc-nds-0886/
[9] R.E. Chrien, et al., Phys. Rev. C**1** (1970) 973.
[10] A.M. Lane and J.E. Lynn, Nucl. Phys. **17** (1960) 563 and 586.

[11] J. Kopecky, A.M.J. Spits and A.M. Lane, Phys. Lett. **49**B (1974) 323.
[12] S.F. Mughabghab "*Atlas of Neutron Resonances*" (Elsevier 2018).
[13] R.E. Chrien and J. Kopecky, Nucl. Phys. A**264** (1976) 63.
[14] J. Kopecky, Photon Strength Functions in Thermal Capture, IAEA report INDC(NDS)-0799, 2020, https://www-nds.iaea.org/publications/indc/indc-nds-0799/
[15] J. Kopecky, Photon Strength Functions in Thermal Capture II, IAEA report INDC(NDS)-0815, 2020, https://www-nds.iaea.org/publications/indc/indc-nds-0815/
[16] J. Kopecky and S. Goriely, The E1 and M1 Upbend in Neutron Capture revisited, IAEA Report INDC(NDS)-0839, 2022 Section 2.4, https://www-nds.iaea.org/publications/indc/indc-nds-0839/
[17] S. Goriely, et al., Phys. Rev. C**98** (2018) 014327.
[18] S. Goriely and V. Plujko, Phys. Rev. C**99** (2019) 014303.
[19] J. Kopecky and M. Uhl, Phys. Rev. C**41** (1990) 1941.
[20] K. Sieja, Europhys. J. Conf. **146** (2017) 05004.
[21] R. Schwengner, et al., Phys. Rev. Lett. **118** (2017) 092502.
[22] B.A. Brown and A.C. Larsen, Phys. Rev. Lett. **113** (2014) 252502.
[23] J. E. Mitbo, et al., Phys. Rev. C**98** (2018) 064321.
[24] J. Kopecky and S. Goriely, Adendum to IAEA(NDS) reports on the neutron capture Photon Strength Functions, IAEA report INDC(NDS)-0821, 2020 Fig. Fig. 14, https://www-nds.iaea.org/publications/indc/indc-nds-0821/
[25] A.C.Larsen, et al., Phys. Rev. C**83** (2011) 034315. https://doi.org/10.1103/PhysRevC.83.034315
[26] A. Schiller, et al., Nucl. Inst. Meth. A**447** (2000) 498.
[27] T. Renstrom, et al., Phys. Rev. C**98** (2018) 054310.
[28] J. Kopecky and F. Becvar, Comparison of Photon Strength Functions from the OSLO Method with Neutron Capture Systematics, IAEA report INDC(NDS)-0868, 2022, https://www-nds.iaea.org/publications/indc/indc-nds-0868/
[29] Tomandl, private communication
[30] C.F. Clement, A.M. Lane and J. Kopecky, Phys. Lett. **71**B (1977) 10.
[31] S. Goriely, priv. communication.

Nuclear Data Section
International Atomic Energy Agency
Vienna International Centre, P.O. Box 100
A-1400 Vienna, Austria

E-mail: nds.contact-point@iaea.org
Fax: (43-1) 26007
Telephone: (43-1) 2600 21725
Web: https://nds.iaea.org